Focus Article

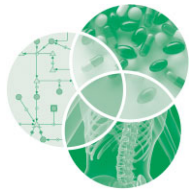

# Electrophysiological models of neural processing

Mark E. Nelson*

**The brain is an amazing information processing system that allows organisms to adaptively monitor and control complex dynamic interactions with their environment across multiple spatial and temporal scales. Mathematical modeling and computer simulation techniques have become essential tools in understanding diverse aspects of neural processing ranging from sub-millisecond temporal coding in the sound localization circuity of barn owls to long-term memory storage and retrieval in humans that can span decades. The processing capabilities of individual neurons lie at the core of these models, with the emphasis shifting upward and downward across different levels of biological organization depending on the nature of the questions being addressed. This review provides an introduction to the techniques for constructing biophysically based models of individual neurons and local networks. Topics include Hodgkin-Huxley-type models of macroscopic membrane currents, Markov models of individual ion-channel currents, compartmental models of neuronal morphology, and network models involving synaptic interactions among multiple neurons.**  *WIREs Syst Biol Med* 2011 3 74–92 DOI: 10.1002/wsbm.95

## INTRODUCTION

Understanding the electrophysiological basis of neural coding, communication, and information processing is central to modern neuroscience research. Mathematical modeling and computer simulation have become an integral part of the neuroscientist's toolbox for exploring these phenomena at a variety of levels of organization, from the biophysical basis of current flow through individual ion channels, to the modeling of aspects of cognitive function arising from the distributed activity of large populations of neurons. Neural models can be constructed at many levels of abstraction. Some types of scientific questions can be addressed using highly reduced models that treat neurons as simple threshold devices, whereas other questions require detailed models of membrane biophysics and intracellular signaling networks.

This article will focus on the tools and techniques for constructing *biophysically detailed compartmental models* of individual neurons and local networks.[1,2] Such models are well positioned to take advantage of emerging neuroinformatics approaches that can potentially link such models with a wealth of empirical data currently being compiled and organized into large neuroscientific databases.[3–5] In contrast, highly abstracted models lack sufficient biological detail to establish meaningful links to these databases, whereas large systems-level models involving multiple brain regions are generally too diverse in structure and function for neuroinformatics approaches to be productive. In the intermediated term over the next several years, biophysically detailed models of single neurons and local networks will likely provide the most fruitful level of analysis for uncovering new functional relationships, dynamical principles, and information-processing strategies.

How do electrophysiological models fit into an informatics approach to neuroscience? This question is perhaps best answered in the context of a bottom-up view of the problem. Starting at the molecular level, sequence-based informatics approaches are being used to reveal information about structural and evolutionary relationships among ion channels and receptor proteins. Molecular dynamics simulations can help establish links from the structural level to the functional properties of individual ion channel and receptor complexes. Electrophysiological models come into play at the next level of organization where

*Correspondence to: m-nelson@illinois.edu

Department of Molecular and Integrative Physiology and The Beckman Institute for Advanced Science and Technology, University of Illinois at Urbana-Champaign, Urbana, IL, USA

DOI: 10.1002/wsbm.95

information-processing properties emerge from the dynamic interactions of multiple channel and receptor types at the single-neuron level and interactions of multiple neurons at the network level.

Neurons typically contain numerous types of ion channels and membrane receptors. Different types of neurons express different combinations of these proteins, with varying densities and varying spatial distributions. There are, for example, dozens of different types of voltage-gated $K^+$ channels, but an individual neuron may only express a few of these, and the expression might be restricted to the soma or to particular regions of the dendrites.[6,7] Different types of $K^+$ channels vary in their electrophysiological properties, such as activation and inactivation voltages, time constants, and conductances. This heterogeneity suggests that $K^+$ channels may be differentially expressed and distributed in order to shape the electrophysiological response properties of individual neurons for carrying out particular types of information-processing tasks.

The contributions of different ion channels to the information-processing capabilities of the system cannot be deduced from the properties of individual ion channels alone. Rather, functional properties at the single-neuron level must be evaluated in the presence of an appropriate mix of channel types, densities, and distributions and in the context of physiologically relevant spatiotemporal patterns of input. For example, certain types of $K^+$ channels from the Kv3 gene family are known to be activated only at rather depolarized membrane potentials and tend to have fast activation and inactivation time constants.[8] Using biophysically detailed compartmental models, neuroscientists have been able to achieve a detailed understanding of how Kv3 channel properties contribute to temporal signal processing in the electric sense of weakly electric fish[9–11] and in the mammalian auditory system.[12] If appropriate databases were available and suitable neuroinformatics tools existed, one could imagine undertaking a variety of interesting comparative investigations regarding the functional role of Kv3 channels in other species, other sensory systems, and other neural information-processing contexts.

## BACKGROUND

This article assumes a general familiarity with the neurophysiological and biophysical mechanisms associated with electrical signaling in neurons. Good introductory material in this area can be found in numerous undergraduate textbooks (e.g., Refs 13 and 14). Recent advanced texts are available that provide detailed, up-to-date coverage in areas such as the cellular and molecular biology of nerve cells (e.g., Ref 15) and the biophysical properties of ion channels (e.g., Ref 16). A brief glossary is provided here as a convenient reference for some of the key terminology and functional concepts.

## Glossary

**action potential** A transient electrical impulse that propagates along an axon and serves as the most common form of electrical signaling between neurons. The duration is typically on the order of a millisecond, and the amplitude is on the order of 100 mV. Action potentials are also called nerve impulses or spikes.

**axon** An output branch of a neuron that conducts action potentials away from the site of initiation and conveys electrical signals to other neurons or effectors. The axon usually starts off as a single long branch but may terminate in a complex branched arbor that distributes outputs to large numbers of target neurons.

**compartmental model** A single-neuron model that divides the cell into multiple spatial compartments. Each compartment can have different properties (length, diameter, membrane voltage, ion channel densities, etc.). The model produces a coupled set of differential equations that are solved using numerical integration techniques.

**conductance** A measure of the ease with which electric current flows through a material; the reciprocal of resistance; conductance units are siemens; conductance (siemens) is a measure of current (amperes) divided by voltage (volts).

**dendrite** An input branch of a neuron that typically receives synaptic contacts from other neurons and conveys graded electrical potentials to other parts of the neuron.

**equilibrium potential** The membrane potential at which the effects of the electrical potential difference and the concentration gradient across the membrane are balanced so as to produce no net ion flux. Also called the Nernst potential. Calculated from the Nernst equation: $E_{\text{ion}} = (RT/zF)\ln([\text{ion}]_{\text{out}}/[\text{ion}]_{\text{in}})$, where $R$ is the universal gas constant, $T$ the temperature in Kelvin, $z$ the ionic charge, $F$ Faraday's constant, and $[\text{ion}]_{\text{in}}$ and $[\text{ion}]_{\text{out}}$ are ionic concentrations.

  

**gating** The process by which ion channels open and close so as to regulate the flow of ions. Voltage-gated ion channels change their gating state based on the local electrical potential difference across the cell membrane. Ligand-gated channels change their gating state based on the binding of signaling molecules (neurotransmitters). Gating usually involves a change in the conformation of the channel protein.

**Hodgkin–Huxley model** A model of the ionic basis of the action potential in squid giant axon developed by Hodgkin and Huxley and published in 1952. More generally, this term can refer to any model that uses a Hodgkin–Huxley (HH)-type mathematical formalism to describe macroscopic ionic currents in nerve cells based on voltage-dependent gating properties.

**macroscopic conductance** The electrical conductance arising from a population of single-channel conductances; often quoted in terms of conductance per unit area of membrane; typically in the range of millisiemens (mS) per square centimeter.

**Markov model** A formalism for modeling stochastic processes which treats the behavior of a system as a series of transitions between distinct states. In the context of ion channels, these distinct states represent different conformational states. Some conformations will correspond to closed states, some to open states, and some to inactivated states.

**membrane potential** The voltage across the cell membrane. If the potential outside of the cell is used as a reference (0 mV), then a typical membrane potential for a neuron at rest would be about −70 mV. The choice of reference point, however, is a matter of convention. In some cases, the inside of the cell is used as a reference, in which case the resting membrane potential would be 0 mV and the external potential would be +70 mV.

**Monte Carlo method** A numerical method for simulating the behavior of a stochastic system by using random numbers to generate possible outcomes based on a model of the underlying probability distribution.

**single-channel conductance** The electrical conductance of a single-ion channel in the open state; typically between 1 and 150 pS (picosiemens).

**soma** The cell body of the neuron; contains the nucleus and much of the metabolic machinery of the cell.

**reversal potential** The membrane potential at which no net current flows through an open ion channel or activated synapse. If the channel or synapse is permeable to a single ionic species, then the reversal potential is equal to the equilibrium potential for that ion. Otherwise, the reversal potential reflects a weighted sum of the equilibrium potentials for all permeant ionic species.

**voltage clamp** A technique for recording the ionic currents across the cell membrane during controlled changes in the membrane potential. Fast feedback circuitry is used to maintain the membrane potential at the desired 'command' level.

## TECHNICAL DETAILS AND METHODOLOGY

### HH Models

The core mathematical framework for modern biophysically based neural modeling was developed half a century ago by Sir Alan Hodgkin and Sir Andrew Huxley. They carried out an elegant series of electrophysiological experiments on the squid giant axon in the late 1940s and early 1950s. The squid giant axon is notable for its extraordinarily large diameter (~0.5 mm). Most axons in the squid nervous system and in other nervous systems are typically at least 100 times thinner. The large size of the squid giant axon is a specialization for rapid conduction of action potentials that trigger the contraction of the squid's mantle when escaping from a predator. In addition to being beneficial for the squid, the large diameter of the giant axon was beneficial for Hodgkin and Huxley because it permitted manipulations that were not technically feasible in smaller axons that had been used in biophysical studies up to that point. In a well-designed series of experiments, Hodgkin and Huxley systematically demonstrated how the macroscopic ionic currents in the squid giant axon could be understood in terms of changes in $Na^+$ and $K^+$ conductances in the axon membrane. Based on a series of voltage-clamp experiments, they developed a detailed mathematical model of the voltage-dependent and time-dependent properties of the $Na^+$ and $K^+$ conductances. The empirical work led to the development of a coupled set of differential equations describing the ionic basis of the action potential,[17] which became known as the HH model. The real predictive power of

  

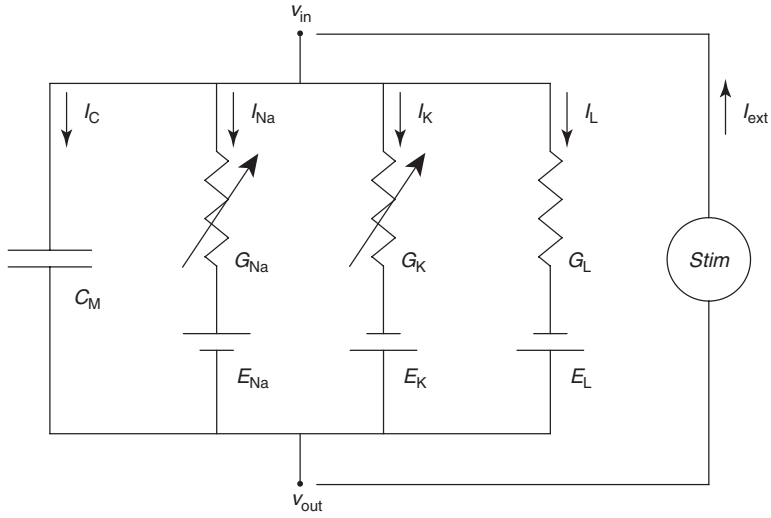


**FIGURE 1** | Electrical equivalent circuit for a short segment of squid giant axon. The capacitor represents the capacitance of the cell membrane; the two variable resistors represent voltage-dependent $Na^+$ and $K^+$ conductances, the fixed resistor represents a voltage-independent leakage conductance, and the three batteries represent reversal potentials for the corresponding conductances. The pathway labeled '*stim*' represents an externally applied current, such as might be introduced via an intracellular electrode. The sign conventions for the various currents are indicated by the directions of the corresponding arrows. Note that the arrow for the external stimulus current $I_{ext}$ is directed from outside to inside (i.e., inward stimulus current is positive), whereas arrows for the ionic currents $I_{Na}$, $I_K$, and $I_L$ are directed from inside to outside (i.e., outward ionic currents are positive). (Adapted with permission from Ref 17. Copyright 1952 John Wiley & Sons, Inc).

the model became evident when Hodgkin and Huxley demonstrated that numerical integration of these differential equations (using a hand-cranked mechanical calculator!) could accurately reproduce all the key biophysical properties of the action potential. For this outstanding achievement, Hodgkin and Huxley were awarded the 1963 Nobel Prize in Physiology and Medicine (shared with Sir John Eccles for his work on the biophysical basis of synaptic transmission).

### *Electrical Equivalent Circuits*

In biophysically based neural modeling, the electrical properties of a neuron are represented in terms of an electrical equivalent circuit. Capacitors are used to model the charge storage capacity of the cell membrane, resistors are used to model the various types of ion channels embedded in membrane, and batteries are used to represent the electrochemical potentials established by differing intra- and extracellular ion concentrations. In their seminal paper on the biophysical basis of the action potential, Hodgkin and Huxley[17] modeled a segment of squid giant axon using an equivalent circuit similar to that shown in Figure 1. In the equivalent circuit, the current across the membrane has two major components, one associated with the membrane capacitance and the other one associated with the flow of ions through resistive membrane channels. The capacitive current $I_c$ is defined by the rate of change of charge $q$ at the membrane surface: $I_c = dq/dt$. The charge $q(t)$ is related to the instantaneous membrane voltage $V_m(t)$ and membrane capacitance $C_m$ by the relationship $q = C_m V_m$. Thus, the capacitive current can be rewritten as $I_c = C_m dV_m/dt$. In the HH model of the squid axon, the ionic current $I_{ion}$ is subdivided into three distinct components: a sodium current $I_{Na}$, a potassium current $I_K$, and a small leakage current $I_L$ that is primarily carried by chloride ions. The behavior of an electrical circuit of the type shown in Figure 1 can be described by a differential equation of the general form:

$$C_m \frac{dV_m}{dt} + I_{ion} = I_{ext} \quad (1)$$

where $I_{ext}$ is an externally applied current, such as might be introduced through an intracellular electrode. Equation (1) is the fundamental equation relating the change in membrane potential to the currents flowing across the membrane.

### *Macroscopic Ionic Currents*

The individual ionic currents $I_{Na}$, $I_K$, and $I_L$ shown in Figure 1 represent the macroscopic currents flowing through a large population of individual ion channels. In HH-style models, the macroscopic current is assumed to be related to the membrane voltage through an Ohm's law relationship of the form $V = IR$. In many cases, it is more convenient to express this relationship in terms of conductance rather than resistance, in which case Ohm's law becomes $I = GV$, where the conductance $G$ is the inverse of resistance, $G = 1/R$. In applying this relationship to ion channels, the equilibrium potential $E_k$ for each ion type also needs to be taken into account. This is the potential at which the net ionic current flowing across the membrane would be zero. The equilibrium potentials are represented by the batteries in Figure 1. The current is proportional to the conductance times the difference between the membrane potential $V_m$ and the equilibrium potential

  

$E_k$. The total ionic current $I_{ion}$ is the algebraic sum of the individual contributions from all participating channel types found in the cell membrane:

$$I_{ion} = \sum_k I_k = \sum_k G_k(V_m - E_k) \quad (2)$$

which expands to the following expression for the HH model of the squid axon:

$$I_{ion} = G_{Na}(V_m - E_{Na}) + G_K(V_m - E_K) + G_L(V_m - E_L) \quad (3)$$

Note that individual ionic currents can be positive or negative depending on whether the membrane voltage is above or below the equilibrium potential. This raises the question of sign conventions. Is a positive ionic current flowing into or out of the cell? The most commonly used sign convention in neural modeling is that ionic current flowing *out* of the cell is positive and ionic current flowing into the cell is negative (see Section on 'Sign Conventions' for more details).

In general, the conductances are not constant values, but can depend on other factors like the membrane voltage or the intracellular calcium concentration. In order to explain their experimental data, Hodgkin and Huxley postulated that $G_{Na}$ and $G_K$ were voltage-dependent quantities, whereas the leakage current $G_L$ was taken to be constant. Thus, the resistor symbols in Figure 1 are shown as variable resistors for $G_{Na}$ and $G_K$, and as a fixed resistor for $G_L$. Today, we know that the voltage-dependence of $G_{Na}$ and $G_K$ can be related to the biophysical properties of the individual ion channels that contribute to the macroscopic conductances. Although Hodgkin and Huxley did not know about the properties of individual membrane channels when they developed their model, it will be convenient for us to describe the voltage-dependent aspects of their model in those terms.

### Gates

The macroscopic conductances of the HH model can be considered to arise from the combined effects of a large number of microscopic ion channels embedded in the membrane. Each individual ion channel can be thought of as containing one or more physical *gates* that regulate the flow of ions through the channel. An individual gate can be in one of two states, *permissive* or *nonpermissive*. When *all* of the gates for a particular channel are in the permissive state, ions can pass through the channel and the channel is *open*. If any of the gates are in the nonpermissive state, ions cannot flow and the channel is *closed*. Although it might seem more natural to speak of *gates* as being *open* or *closed*, a great deal of confusion can be avoided by consistently using the terminology *permissive* and *nonpermissive* for gates while reserving the terms *open* and *closed* for channels.

The voltage-dependence of ionic conductances is incorporated into the HH model by assuming that the probability for an individual gate to be in the permissive or nonpermissive state depends on the value of the membrane voltage. If we consider gates of a particular type $i$, we can define a probability $p_i$, ranging between 0 and 1, which represents the *probability* of an individual gate being in the permissive state. If we consider a large number of channels, rather than an individual channel, we can also interpret $p_i$ as the fraction of gates in that population that are in the permissive state. At some point in time $t$, let $p_i(t)$ represent the fraction of gates that are in the permissive state. Consequently, $1 - p_i(t)$ must be in the nonpermissive state.

$$\text{fraction in nonpermissive state, } 1 - p_i\,(t) \quad \underset{\beta_i(V)}{\overset{\alpha_i(V)}{\rightleftharpoons}} \quad \text{fraction in permissive state, } p_i\,(t)$$

The rate at which gates transition from the nonpermissive state to the permissive state is denoted by a variable $\alpha_i(V)$, which has units of 1/s. Note that this 'rate constant' is not really constant, but depends on membrane voltage $V$. Similarly, there is a second rate constant, $\beta_i(V)$, describing the transition rate from the permissive to the nonpermissive state. Transitions between permissive and nonpermissive states in the HH model are assumed to obey first-order kinetics:

$$\frac{dp_i}{dt} = \alpha_i(V)(1 - p_i) - \beta_i(V)p_i \quad (4)$$

where $\alpha_i(V)$ and $\beta_i(V)$ are voltage-dependent. If the membrane voltage $V_m$ is clamped at some fixed value $V$, then the fraction of gates in the permissive state will eventually reach a steady-state value (i.e., $dp_i/dt = 0$) as $t \to \infty$ given by

$$p_{i,t\to\infty} = \frac{\alpha_i(V)}{\alpha_i(V) + \beta_i(V)} \quad (5)$$

The time course for approaching this equilibrium value is described by a simple exponential with time constant $\tau_i(V)$ given by:

$$\tau_i(V) = \frac{1}{\alpha_i(V) + \beta_i(V)} \quad (6)$$

  

When an individual channel is open, it contributes some small, fixed value to the total conductance and zero otherwise. The macroscopic conductance for a large population of channels is thus proportional to the number of channels in the open state, which is, in turn, proportional to the probability that the associated gates are in their permissive state. Thus, the macroscopic conductance $G_k$ due to channels of type $k$, with constituent gates of type $i$, is proportional to the *product* of the individual gate probabilities $p_i$:

$$G_k = \bar{g}_k \prod_i p_i \tag{7}$$

where $\bar{g}_k$ is a normalization constant that determines the maximum possible conductance when all the channels are open (i.e., all gates are in the permissive state).

We have presented Eqs. (4)–(7) using a generalized notation that can be applied to a wide variety of conductances beyond those found in the squid axon. To conform to the standard notation of the HH model, the probability variable $p_i$ in Eqs. (4)–(7) is replaced by a variable that represents the gate type. For example, Hodgkin and Huxley modeled the sodium conductance using three gates of a type labeled '$m$' and one gate of type '$h$'. Applying Eq. (7) to the sodium channel using both the generalized notation and the standard notation yields:

$$G_{\mathrm{Na}} = \bar{g}_{\mathrm{Na}} p_m^3 p_h = \bar{g}_{\mathrm{Na}} m^3 h \tag{8}$$

Similarly, the potassium conductance is modeled with four identical '$n$' gates:

$$G_{\mathrm{K}} = \bar{g}_{\mathrm{K}} p_n^4 = \bar{g}_{\mathrm{Na}} n^4 \tag{9}$$

Summarizing the ionic currents in the HH model in standard notation, we have

$$I_{\mathrm{ion}} = \bar{g}_{\mathrm{Na}} m^3 h (V_{\mathrm{m}} - E_{\mathrm{Na}}) + \bar{g}_{\mathrm{K}} n^4 (V_{\mathrm{m}} - E_{\mathrm{K}}) + g_{\mathrm{L}} (V_{\mathrm{m}} - E_{\mathrm{L}}) \tag{10}$$

$$\frac{\mathrm{d}m}{\mathrm{d}t} = \alpha_m(V)(1-m) - \beta_m(V)m \tag{11}$$

$$\frac{\mathrm{d}h}{\mathrm{d}t} = \alpha_h(V)(1-h) - \beta_h(V)h \tag{12}$$

$$\frac{\mathrm{d}n}{\mathrm{d}t} = \alpha_n(V)(1-n) - \beta_n(V)n \tag{13}$$

To completely specify the model, the one task that remains is to specify how the six rate constants in Eqs. (11)–(13) depend on the membrane voltage. Then Eqs. (10)–(13), together with Eq. (1), completely specify the behavior of the membrane potential $V_{\mathrm{m}}$ in the HH model of the squid giant axon.

### *Sign Conventions*

Note that the appearance of $I_{\mathrm{ion}}$ on the left-hand side of Eq. (1) and $I_{\mathrm{ext}}$ on the right indicates that they have opposite *sign conventions*. As the equation is written, a positive external current $I_{\mathrm{ext}}$ will tend to depolarize the cell (i.e., make $V_{\mathrm{m}}$ more positive) while a positive ionic current $I_{\mathrm{ion}}$ will tend to hyperpolarize the cell (i.e., make $V_{\mathrm{m}}$ more negative). This sign convention for ionic currents is sometimes referred to as the neurophysiological or physiologists' convention. This convention is conveniently summarized by the phrase 'inward negative', meaning that an inward flow of positive ions into the cell is considered a negative current. This convention perhaps arose from the fact that when one studies an ionic current in a voltage-clamp experiment, rather than measuring the ionic current directly, one actually measures the clamp current that is necessary to counterbalance it. Thus, an inward flow of positive ions is observed as a negative-going clamp current, hence explaining the 'inward negative' convention. Some neural simulation software packages, such as GENESIS, use the opposite sign convention (inward positive), because that allows all currents to be treated consistently. In the figures shown in this article, membrane currents are plotted using the neurophysiological convention (inward negative).

### *Voltage Conventions*

Although we are on the topic of *conventions*, there are two more issues that should be discussed here. The first concerns the *value* of the membrane potential $V_{\mathrm{m}}$. Recall that potentials are relative; only potential differences can be measured directly. Thus, when defining the intracellular potential $V_{\mathrm{m}}$, one is free to choose a convention that defines the resting intracellular potential to be zero (the convention used by Hodgkin and Huxley), or one could choose a convention that defines the extracellular potential to be zero, in which case the resting intracellular potential would be around −70 mV. In either case, the potential *difference* across the membrane is the same, it is simply a matter of how 'zero' is defined. Most simulation software packages allow the user to select a voltage reference convention they like.

The second convention we need to discuss concerns the *sign* of the membrane potential. The modern convention is that depolarization makes the membrane potential $V_{\mathrm{m}}$ more positive. However, Hodgkin and Huxley[17] used the opposite sign convention (depolarization negative) in their article.

  

In the figures in this article, we use the modern convention that depolarization is positive.

At a conceptual level, the choice of conventions for currents and voltages is inconsequential; however, at the implementation level it matters a great deal, because inconsistencies will cause the model to behave incorrectly. The most important thing in choosing conventions is to ensure that the choices are internally consistent. One must pay careful attention to these issues when implementing a simulation using equations from a published model, because it may be necessary to convert the empirical results reported using one set of conventions into a form that is consistent with one's own model conventions.

### *Rate Constants*

How did Hodgkin and Huxley go about determining the voltage-dependence of the rate constants $\alpha$ and $\beta$ that appear in Eqs. (11)–(13)? How did they determine that the potassium conductance should be modeled with four $n$ gates, but that the sodium conductance required three $m$ gates and one $h$ gate? In order to answer these questions, we need to look in more detail at the type of data that can be obtained from voltage-clamp experiments.

Figure 2 shows simulated voltage-clamp data, similar to those obtained by Hodgkin and Huxley in their studies of squid giant axon. In these experiments, Hodgkin and Huxley used voltage-clamp circuitry to step the membrane potential from the resting level (0 mV) to a steady depolarized level. The figure shows the time course of the change in normalized $K^+$ conductance for several different voltage steps. Three qualitative effects are apparent in the data. First, the steady-state conductance level increases with increasing membrane depolarization. Second, the onset of the conductance change becomes faster with increasing depolarization. Third, there is a slight temporal delay between the start of the voltage step and the change in conductance.

In the simulated voltage-clamp experiments illustrated in Figure 2, the membrane potential starts in the resting state ($V_m = 0$, using the HH voltage convention) and is then instantaneously stepped to a new clamp voltage $V_c$. What is the time course of the state variable $n$, which controls gating of the $K^+$ channel, under these circumstances? Recall that the differential equation governing the state variable $n$ is given by:

$$\frac{dn}{dt} = \alpha_n(V)(1-n) - \beta_n(V)n \qquad (14)$$

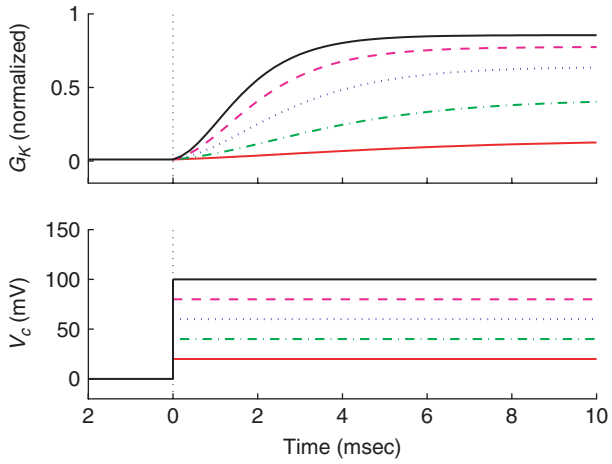


**FIGURE 2** | Simulated voltage-clamp data illustrating voltage-dependent properties of the $K^+$ conductance in squid giant axon. The command voltage $V_c$ (mV) is shown in the lower panel, and the $K^+$ current is shown in the upper panel. Simulation parameters are from the HH model.[17]

Initially, with $V_m = 0$, the state variable $n$ has a steady-state value (i.e., when $dn/dt = 0$) given by Eq. (5):

$$n_\infty(0) = \frac{\alpha_n(0)}{\alpha_n(0) + \beta_n(0)} \qquad (15)$$

When $V_m$ is clamped to a new level $V_c$, the gating variable $n$ will eventually reach a new steady-state value given by

$$n_\infty(V_c) = \frac{\alpha_n(V_c)}{\alpha_n(V_c) + \beta_n(V_c)} \qquad (16)$$

The solution to Eq. (14) that satisfies these boundary conditions is a simple exponential of the form:

$$n(t) = n_\infty(V_c) - (n_\infty(V_c) - n_0(0))e^{-t/\tau_n(V_c)} \qquad (17)$$

Given Eq. (17), which describes the time course of $n$ in response to a step change in command voltage, one could try fitting curves of this form to the conductance data shown in Figure 2 by finding the values of $n_\infty(V_c)$, $n_\infty(0)$, and $\tau_n(V_c)$ that give the best fit to the data for each value of $V_c$. Figure 3 illustrates this process, using some simulated conductance data generated by the HH model. Recall that $n$ takes on values between 0 and 1, so in order to fit the conductance data, $n$ must be multiplied by a normalization constant $\bar{g}_K$ that has units of conductance. For simplicity, the normalized conductance $G_K/\bar{g}_K$ is plotted. The dotted line in Figure 3 shows the best-fit results for a simple exponential curve of the form given in Eq. (17). Although this simple form does a reasonable job of

  

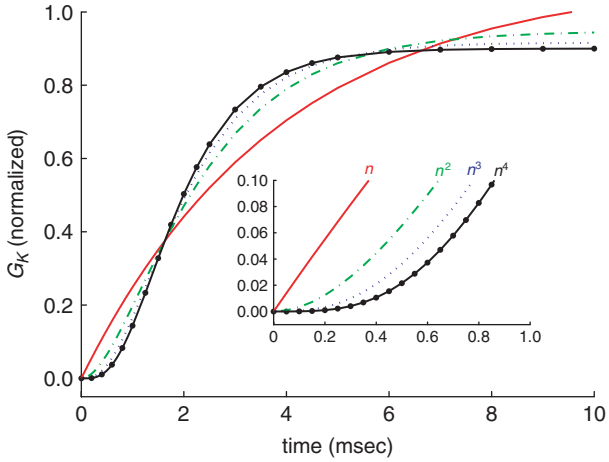


**FIGURE 3** | Best-fit curves of the form $G_k = \bar{g}_K n^j$ ($j = 1$–4) for simulated conductance versus time data. The inset shows an enlargement of the first millisecond of the response. The initial inflection in the curve cannot be well-fit by a simple exponential (dotted line) which rises linearly from zero. Successively higher powers of $j$ ($j = 2$: dot–dashed; $j = 3$: dashed line) result in a better fit to the initial inflection. In this case, $j = 4$ (solid line) gives the best fit.

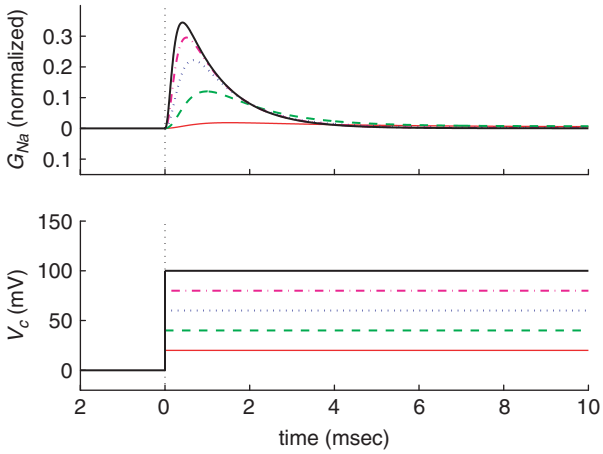


**FIGURE 4** | Simulated voltage-clamp data illustrating activation and inactivation properties of the $Na^+$ conductance in squid giant axon. The command voltage $V_c$ is shown in the lower panel, and the $Na^+$ current is shown in the upper panel. Simulation parameters are from the HH model.[17]

capturing the general time course of the conductance change, it fails to reproduce the sigmoidal shape and the temporal delay in onset. This discrepancy is most apparent near the onset of the conductance change, shown in the inset of Figure 3. Hodgkin and Huxley realized that a better fit could be obtained if they considered the conductance to be proportional to a higher power of $n$. Figure 3 shows the results of fitting the conductance data using a form $G_K = \bar{g}_k n^j$ with powers of $j$ ranging from 1 to 4. Using this sort of fitting procedure, Hodgkin and Huxley determined that a reasonable fit to the $K^+$ conductance data could be obtained using an exponent of $j = 4$. Thus, they arrived at a description for the $K^+$ conductance under voltage-clamp conditions given by:

$$G_K = \bar{g}_K n^4 = \bar{g}_K \left[n_\infty(V_c) - (n_\infty(V_c) - n_\infty(0))e^{-t/\tau_n}\right]^4 \quad (18)$$

### *Activation and Inactivation Gates*

The strategy that Hodgkin and Huxley used for modeling the sodium conductance is similar to that described above for the potassium conductance, except that the sodium conductance shows a more complex behavior. In response to a step change in clamp voltage, the sodium conductance exhibits a transient response (Figure 4), whereas the potassium conductance exhibits a sustained response (Figure 2). Sodium channels inactivate whereas the potassium channels do not. To model this process, Hodgkin and Huxley postulated that the sodium channels had two types of gates, an activation gate, which they labeled $m$, and an inactivation gate, which they labeled $h$. Again, boundary conditions dictated that $m$ and $h$ must follow a time course given by

$$m(t) = m_\infty(V_c) - (m_\infty(V_c) - m_\infty(0))e^{-t/\tau_m(V_c)} \quad (19)$$

$$h(t) = h_\infty(V_c) - (h_\infty(V_c) - h_\infty(0))e^{-t/\tau_h(V_c)} \quad (20)$$

Hodgkin and Huxley made some further simplifications by observing that the sodium conductance in the resting state is small compared with the value obtained during a large depolarization; hence, they were able to neglect $m_\infty(0)$ in their fitting procedure. Likewise, steady-state inactivation is nearly complete for large depolarizations, so $h_\infty(V_c)$ could also be eliminated from the fitting procedure. With these simplifications, Hodgkin and Huxley were able to fit the remaining parameters from the voltage-clamp data. The sodium conductance $G_{Na}$ was thus modeled by an expression of the form $G_{Na} = \bar{g}_{Na} m^3 h$.

### *Parameterizing the Rate Constants*

By fitting voltage-clamp data as discussed above, steady-state conductance values and time constants can be empirically determined as a function of command voltage for each of the gating variables associated with a particular channel. Using Eqs. (5) and (6), the steady-state conductance values and time constants can be transformed into expressions for the forward and backward rate constants $\alpha$ and $\beta$.

  

For example, for the potassium channel $n$ gate we have

$$\alpha_n(V) = \frac{n_\infty(V)}{\tau_n(V)} \tag{21}$$

$$\beta_n(V) = \frac{1 - n_\infty(V)}{\tau_n(V)} \tag{22}$$

Thus, there are two equivalent representations for the voltage-dependence of a channel. One representation specifies the voltage-dependence of the rate constants, which we will call the $\alpha/\beta$ representation. The other representation specifies the voltage-dependence of the steady-state conductance and the time constant, which we will call the $n_\infty/\tau$ representation. These two representations are interchangeable, and one can easily convert between them using the algebraic relationships in Eqs. (5) and (6) (for transforming from $\alpha/\beta$ to $n_\infty/\tau$) and Eqs. (21) and (22) (for transforming from $n_\infty/\tau$ to $\alpha/\beta$). In general, experimentalists tend to use the $n_\infty/\tau$ representation because it maps more directly onto the results of voltage-clamp experiments. Modelers, on the other hand, tend to express voltage-dependences using the $\alpha/\beta$ representation, because it maps more directly onto the gating Eqs. (11)–(13) in the standard formulation of the HH model.

Voltage-clamp experiments yield estimates of $n_\infty/\tau$ or $\alpha/\beta$ only at the discrete clamp voltages $V_c$ used in the experiment. Numerical integration of the HH model, however, requires that $n_\infty/\tau$ or $\alpha/\beta$ values be specified over a continuous range of membrane voltages, because the membrane potential varies continuously in the model. Typically, voltage-dependences are expressed as a continuous function of voltage, and the task for the modeler becomes one of determining the parameter values that best fit the data. As an illustration, the closed circles in Figure 5a and b represent empirical data on $n_\infty(V_c)$ and $\tau_n(V_c)$ obtained by Hodgkin and Huxley (Table 1 of Hodgkin and Huxley[17]). The data points in Figure 5c and d show the same data set transformed into the $\alpha/\beta$ representation. Hodgkin and Huxley used the following functional forms to parameterize their $K^+$ conductance results (shown as solid lines in Figure 5):

$$\alpha_n(V) = \frac{0.01\,(10 - V)}{\exp\,(10 - V/10) - 1} \tag{23}$$

$$\beta_n(V) = 0.125 \exp\left(\frac{-V}{80}\right) \tag{24}$$

If Eqs. (23) and (24) above are compared with Eqs. (12) and (13) from the original article,[17] you will note that the sign of the membrane voltage has been changed to correspond to the modern convention (see Section on 'Voltage Conventions' above). Hodgkin and Huxley used similar functional forms to describe the voltage-dependence of the $m$ and $h$ gates of the sodium channel:

$$\alpha_m(V) = \frac{0.1\,(25 - V)}{\exp\,(25 - V/10) - 1} \tag{25}$$

$$\beta_m(V) = 4 \exp\left(\frac{-V}{18}\right) \tag{26}$$

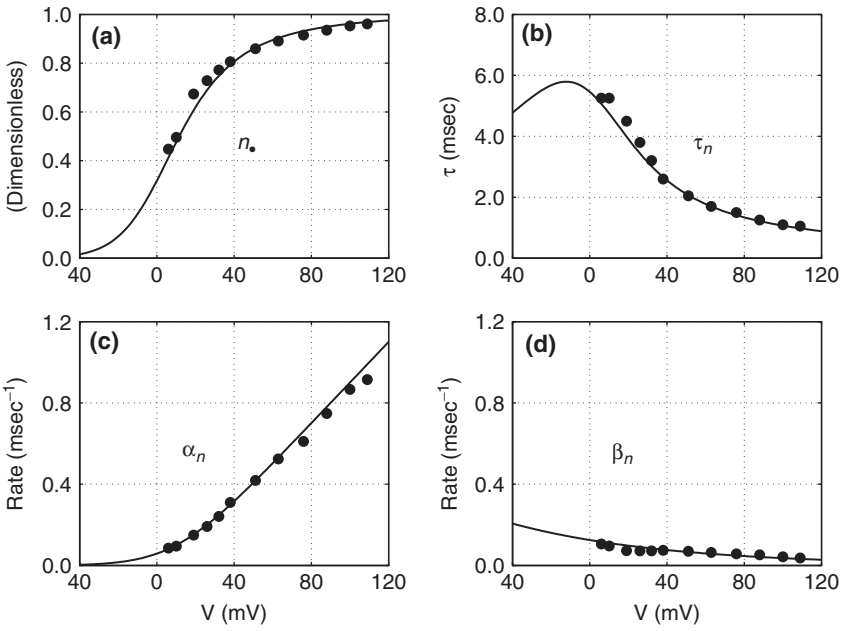


**FIGURE 5** | Parametric fits to voltage-dependence of the $K^+$ conductance in the HH model. (A) Steady-state value $n_\infty$; (B) time constant $\tau_n$ (C) forward rate constant $\alpha_n$; and (D) backward rate constant $\beta_n$. Data points are from Table 1 of Hodgkin and Huxley.[17] Solid lines in panels (C) and (D) are parametric fits to the rate data. The best-fit curves correspond to Eqs. (23) and (24), respectively. Solid lines in panels (A) and (B) are the transformations of the $\alpha/\beta$ functions into the $n_\infty/\tau$ representation using Eqs. (5) and (6).

  

$$\alpha_h(V) = 0.07 \exp\left(\frac{-V}{20}\right) \quad (27)$$

$$\beta_h(V) = \frac{1}{\exp(30 - V/10) + 1} \quad (28)$$

In neural simulation software packages, the rate constants in HH-style models are often parameterized using a generic functional form:

$$\alpha(V) = \frac{A + BV}{C + H \exp(V + D/F)} \quad (29)$$

In general, this functional form may require up to six parameters ($A$, $B$, $C$, $D$, $F$, and $H$) to fully specify the rate equation. However, in many cases, adequate fits to the data can be obtained using far fewer parameters. Fortunately, Eq. (29) is flexible enough that it can be transformed into simpler functional forms by setting certain parameters to either 0 or 1. For example, if the voltage-clamp data can be adequately fit by an exponential function over the relevant range of voltages, then setting $B = 0, C = 0, D = 0$, and $H = 1$ in Eq. (29), results in a simple exponential form, $a(V) = A \exp(-V/F)$, with just two free parameters ($A$ and $F$) to be fit to the data. Similarly, setting $B = 0$, $C = 1$, and $H = 1$ gives a sigmoidal function with three free parameters ($A$, $D$, and $F$).

One other technical note is that certain function forms can become indeterminate at certain voltage values. For example, the expression for $\alpha_n(V)$ in Eq. (23) evaluates to the indeterminate form 0/0 at $V = 10$. The solution to this problem is to apply L'Hôpital's rule, which states that if $f(x)$ and $g(x)$ approach 0 as $x$ approaches $a$, and $f'(x)/g'(x)$ approaches $L$ as $x$ approaches $a$, then the ratio $f(x)/g(x)$ approaches $L$ as well. Using this rule, it can be shown that $\alpha_n(10) = 0.1$. When implementing HH-style rate functions in computer code, care must be taken to handle such cases appropriately.

### *Calcium-Dependent Channels*

Certain types of ion channels are influenced by both membrane voltage and intracellular calcium concentration. Although calcium-dependence was not part of the original HH model, it is straightforward to extend the HH framework to handle this case. Calcium-dependence is typically implemented by modifying the $\alpha/\beta$ rate equations to include an additional state variable representing the intracellular calcium concentration. For example, Traub[18] proposed a model of intrinsic bursting in hippocampal neurons that included a slow calcium-dependent potassium conductance $G_s$. This conductance was modeled using an HH-style rate equation that depends on both membrane voltage $V$ and intracellular calcium concentration $\chi$. Traub[18] modeled the slow potassium conductance as $G_s = \bar{g}_s q$, where $q$ is a standard HH gating variable with first-order kinetics:

$$\frac{dq}{dt} = \alpha_q(1 - q) - \beta_q q \quad (30)$$

The voltage- and calcium-dependence were incorporated into the rate equations as follows:

$$\alpha_q(\chi, V) = \exp\left(\frac{V}{27}\right) \frac{0.005(200 - \chi)}{\exp(200 - \chi/20) - 1} \quad (31)$$

$$\beta_q = 0.002 \quad (32)$$

Conductances that depend on both membrane voltage and calcium concentration are rarely as well characterized experimentally as are ordinary voltage-dependent channels. In part this is due to the technical challenges in trying to achieve a 'calcium clamp' to precisely quantify the calcium-dependence. Furthermore, voltage-clamp experiments on these conductances are more difficult to interpret because even though the membrane voltage is held fixed by the clamp circuitry, the intracellular calcium concentration is varying during the clamp. Consequently, modelers must often devise rate equations for such channels based on more qualitative criteria than are used for regular voltage-dependent channels. To simplify this task, it is common to take one of the $\alpha/\beta$ rate equations as a constant [as was done for $\beta_q$ in Eq. (32) above] and to put all of the voltage- and calcium-dependence into the other rate equation. This reduces the number of unknown parameters in the model, and it simplifies searching the parameter space.

For understanding the effects on channel gating, the region of space in which the calcium concentration must be known is a thin shell just inside the membrane surface. The calcium concentration in this region can be significantly different from the bulk concentration in the interior of the cell. Calcium enters this shell region primarily through the influx of $Ca^{2+}$ ions through membrane calcium channels. Calcium leaves the shell region because of diffusion and buffering. A simple model of intracellular calcium dynamics describes this process by a differential equation of the form[18]:

$$\frac{d\chi}{dt} = AI_{Ca} - B\chi \quad (33)$$

where $A$ is a constant related to the volume of the shell and the conversion of coulombs to moles of ions, while $B$ is a rate constant representing the

  

effects of diffusion and buffering. As a technical note, recall that ionic currents are typically defined as 'inward negative' (see Section on 'Sign Conventions' above). Using this convention, the constant $A$ in Eq. (33) will be a negative number, such that inward (negative) calcium current will cause a positive change in calcium concentration $\chi$. For a discussion of more advanced techniques for modeling calcium dynamics, see Ref 19.

## Markov Models of Individual Channels

The HH framework has been extremely successful for developing quantitative models of macroscopic currents observed in single neurons. However, a different approach must be used if one is interested in modeling the currents flowing through individual channels. At the microscopic level, gating of individual ion channels is a stochastic process. Transitions between permissive and nonpermissive gating states take place by probabilistic transitions between different conformational states of the ion channel complex. Certain conformational states allow ions to move through the channel, while others do not. When monitored experimentally in single-channel patch-clamp recordings, for example, individual channels are observed to fluctuate randomly between open and closed states.

Markov models provide a framework for describing the microscopic currents through individual ion channels.[20] The basic assumption underlying the Markov model formalism is that the opening and closing of ion channels can be described as a series of transitions between distinct conformational states. Certain states may correspond to the channel being open, closed, inactivated, and so on. Transitions between different states occur according to a set of transition probabilities. Figure 6 shows a generic Markov model consisting of 5 states $S_i$ and 10 transition probabilities $p_{ij}$. Note that the number of transition probabilities will depend on the topology of the Markov model. For example, a fully connected five-state model, in which any state could transition to any other state, would have 20 transition probabilities. Part of the task of designing a Markov model involves determining how many states are involved, which transitions are allowed, and which are forbidden. The forbidden transitions do not appear in the diagram. The modeler's task then becomes one of determining values for the remaining allowed transition probabilities.

The probability to find the system in state $S_i$ at some time $t$ is defined as $P_i(t)$. The transition probability $p_{ij}$ is the conditional probability of finding the system in a new state $j$ if it has recently been in state $i$. The time evolution of $P_i(t)$ can be written as:

$$\frac{dP_i(t)}{dt} = \sum_{j=1}^{n} P_j(t)p_{ji} - \sum_{j=1}^{n} P_i(t)p_{ij} \qquad (34)$$

The first term on the right-hand side of this equation represents the increase in probability of finding the system in state $S_i$ because of transitions entering this state from other states. The second term represents the decrease in probability because of transitions out of state $S_i$ into other states. If there is a large population of identical channels, then $P_i(t)$ can be interpreted as the fraction of channels in state $S_i$ and the transition probabilities $p_{ij}$ can be interpreted as rate constants. Thus, Markov models provide a convenient formalism for linking the gating properties of individual channels to the behavior of macroscopic currents as described by the HH model.

Figure 7a shows a five-state Markov model that corresponds to the $n^4$ gating kinetics of the HH $K^+$ channel model. The Markov model has five distinct states, $n_0$–$n_4$, where the subscript represents the number of HH gates in the permissive state. When the channel is in state $n_1$, for example, one of the gates is in the permissive configuration and three of the gates are nonpermissive. Ions can flow through the channel only when all gates are in the permissive state (state $n_4$); all other states correspond to closed states. The transition probabilities between states can be calculated from the forward ($\alpha_n$) and reverse ($\beta_n$) rate constants of the HH $K^+$ channel model and the assumption that each gate behaves independently. There are four possible ways that the $n_0$ state can transition to the $n_1$ state, so the corresponding transition rate is $4\alpha_n$. The full set

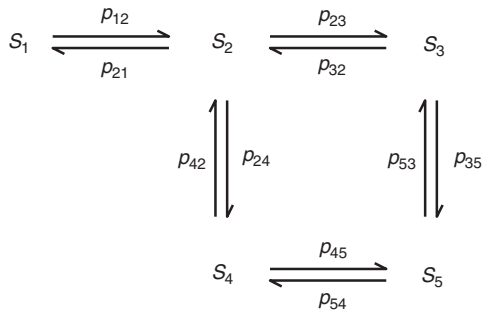


**FIGURE 6** | A representative Markov model diagram. This particular model has five distinct states $S_1$–$S_5$ and 10 transition probabilities $p_{ij}$. In Markov models of ion channels, each state represents a putative conformational state of the ion channel complex. Some conformations will correspond to closed states, some to open states, and some to inactivated states.

  

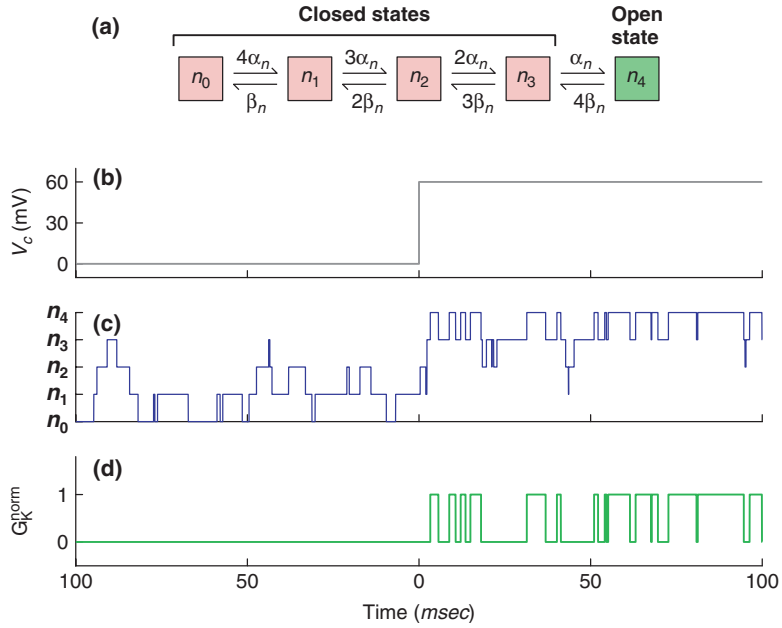


**FIGURE 7** | A Markov model of the HH $K^+$ conductance. (a) The Markov model has four closed states $n_0 - n_3$ and one open state $n_4$. The subscript corresponds to the number of $n$ gates in the permissive state. (b) Command voltage in a simulated voltage-clamp experiment. (c) Monte Carlo simulation of state transitions of the Markov model in response to a step change in command voltage. (d) Normalized conductance of the $K^+$ channel. The channel is open ($G_K^{norm} = 1$) whenever the system is in state $n_4$, otherwise the channel is closed ($G_K^{norm} = 0$).

of transition probabilities that correspond to the HH model kinetics are shown in the figure.

The sequence of openings and closings of an individual channel can be simulated using Monte Carlo techniques to randomly generate state transitions with the specified probabilities. Recall that the HH rate constants are voltage-dependent, so a change in membrane voltage (Figure 7b) will result in a shift of all the transition probabilities and hence a shift in the probability distribution of states. Figure 7c shows a Monte Carlo simulation of the time history of state transitions before and after a step change in clamp voltage. When the membrane is clamped to the resting voltage ($V_C = 0$), the system spends most of its time in states $n_0 - n_2$, which are all closed states. When the membrane is clamped to a depolarized voltage ($V_C = 60$), the system spends most of its time in states $n_2 - n_4$. The channel is open whenever the model is in state $n_4$, as reflected in the conductance record shown in Figure 7d.

Figure 8a shows an eight-state Markov model that corresponds to the $m^3h$ gating kinetics of the HH $Na^+$ channel. The model is in the open state only when all gates are permissive (state $m_3h_1$). Any state in which the inactivation gate is nonpermissive ($h_0$) corresponds to an inactivated state of the channel. According to the HH model, the behavior of the inactivation gate ($h$) is independent of the three activation gates ($m$). This is reflected in the Markov model by the fact that transitions to an inactivated state can potentially occur from any open or closed state. However, careful experimental studies of $Na^+$ channel gating kinetics have revealed that activation and inactivation processes are not completely independent. Figure 8b shows a more recent Markov model of $Na^+$ channel gating[21] that provides a better description of the data.

## Synaptic Models

Thus far, the techniques in this article have focused primarily on modeling voltage-dependent channels. Equally important from a functional perspective are the ligand-gated channels that mediate chemical synaptic transmission. When an action potential arrives at the presynaptic terminal of a chemical synapse, neurotransmitter is released into the synaptic cleft. Neurotransmitter molecules subsequently bind to ligand-gated receptors in the postsynaptic membrane, causing changes in ionic current flow across the membrane. In an equivalent electrical circuit model (Figure 1), ligand-gated channels are represented by additional resistive pathways across the membrane.

For simulating synaptic activation in neural models, the details of synaptic release, diffusion, and receptor binding are often abstracted into a simpler form that describes the postsynaptic conductance as a time-dependent function. The arrival of an action potential at a synapse at time $t_{spike}$ gives rise to a transient change in a postsynaptic conductance that is often modeled using the alpha function[22]:

$$G_{syn}(t) = \frac{g_{peak}e}{\tau_{syn}}(t - t_{spike})e^{-(t-t_{spike})/\tau_{syn}} \quad \text{for } t \geq t_{spike} \tag{35}$$

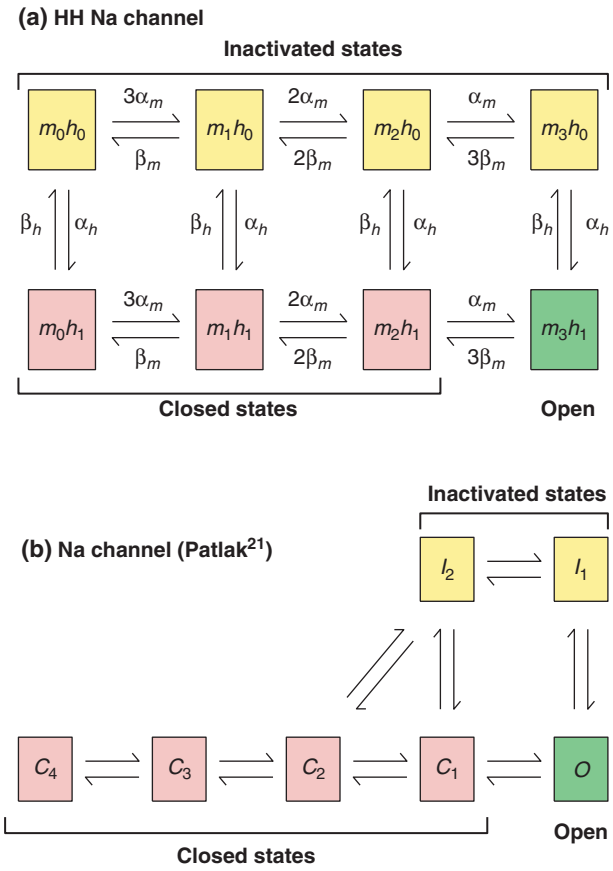


**FIGURE 8** | Two different Markov models of the $Na^+$ conductance. (a) The Markov model corresponding to independent activation and inactivation gating of the HH model has eight distinct states. The subscripts on the states represent the number of gates of each type in the permissive state. The channel is open only when all three $m$ gates and the $h$ gate are in the permissive state ($m_3h_1$). (b) A model proposed by Patlak[21] which includes interactions between the activation and inactivation gates. This model provides a better description of actual voltage-clamp data from squid axon than does the HH model.

The peak of the conductance change occurs at time $t = t_{\text{spike}} + \tau_{\text{syn}}$, and the conductance value at this time is $g_{\text{peak}}$. The synaptic current $I_{\text{syn}}$ associated with the synapse is modeled by $I_{\text{syn}}(t) = G_{\text{syn}}(t)(V - E_{\text{syn}})$, where $E_{\text{syn}}$ is the reversal potential of the synapse.

When a synapse is activated by a sequence of action potentials, the net change in conductance is often modeled as a linear summation of the contributions from each individual action potential. A straightforward implementation based on Eq. (35) would require keeping a time history of spike activity and summating over all previous spike times. However, this approach is computationally inefficient and rarely used in large-scale simulations. There are more efficient methods involving either the reformulation of the conductance change as a second-order differential equation[23] or reorganization of the computation to require the storage of only two running sums per synapse, rather than a complete time history of activation.[24]

Another technique for modeling synaptic conductances utilizes a Markov model approach.[25] The simplest form of such models involves only a single open state and a single closed state. Such two-state models can be represented by:

$$C + T \underset{\beta}{\overset{\alpha}{\rightleftharpoons}} O \tag{36}$$

where $C$ is a closed state, $O$ an open state, $T$ represents neurotransmitter, and $\alpha$ and $\beta$ are forward and backward rate constants, respectively. Unlike the Hodgkin and Huxley model, the rate constants, $\alpha$ and $\beta$, are independent of membrane voltage. Let the fraction of receptors in the open state be represented by $r$, and let the neurotransmitter concentration be denoted by $[T]$. Then the first-order kinetic equation for this system is

$$\frac{dr}{dt} = \alpha[T](1 - r) - \beta r \tag{37}$$

One simple way to model the neurotransmitter concentration is to assume that a constant amplitude pulse of transmitter is released when the action potential arrives at the presynaptic terminal, in which case Eq. (37) can be solved analytically for $r(t)$.[26] The synaptic current is then modeled by:

$$I_{\text{syn}}(t) = \bar{g}_{\text{syn}} r(t)(V - E_{\text{syn}}) \tag{38}$$

In general, Markov models of this type can be much more sophisticated than the two-state model presented above. These more detailed models can have multiple states representing various open, closed, and desensitized configurations. Such biophysically rich Markov models may be particularly useful when using a neuroinformatics approach to investigate how receptor properties are altered by variations in the molecular structure and subunit composition of particular ligand-gated receptors.

### *Metabotropic Receptors*

Up to this point, we have been discussing ionotropic receptors for which neurotransmitter binding causes direct and immediate gating of an associated ion channel. Metabotropic receptors, on the other hand, exert their influence indirectly by acting through an intracellular second messenger system. For metabotropic receptors, neurotransmitter binding

  

leads to the activation of intracellular biochemical pathways, which may ultimately link to the opening or closing of second messenger gated ion channels. The cascade of reactions that take place in such systems can be modeled using a combination of Markov models for the components that have discrete states and standard biochemical reaction kinetics for describing chemical concentrations that vary continuously.[26] For example, the binding of transmitter $T$ to a metabotropic receptor $R$, leading to the formation of an activated receptor state $R^*$, might be described by a two-state Markov model:

$$R + T \underset{\longleftarrow}{\longrightarrow} R^* \tag{39}$$

Following receptor activation, there could be several intermediate biochemical reactions of the general form:

$$A + B \underset{\beta}{\overset{\alpha}{\rightleftarrows}} X + Y \tag{40}$$

which can be modeled using standard reaction kinetics.[27] In Eq. (40), $\alpha$ and $\beta$ are forward and backward rate constants for the reaction. The chemical concentrations are governed by a rate equation of the form:

$$\frac{\mathrm{d}[A]}{\mathrm{d}t} = -\alpha[A][B] + \beta[X][Y] \tag{41}$$

and a set of relationships that reflect the stoichiometry of the reaction

$$\frac{\mathrm{d}[A]}{\mathrm{d}t} = \frac{\mathrm{d}[B]}{\mathrm{d}t} = -\frac{\mathrm{d}[X]}{\mathrm{d}t} = -\frac{\mathrm{d}[Y]}{\mathrm{d}t} \tag{42}$$

In a second messenger cascade, one of the reactants appearing on the left-hand side of one of the biochemical reactions would be the activated receptor $R^*$, and one of the products appearing on the right-hand side would be a second messenger $Z$ that could serve as a ligand for a postsynaptic ion channel. The gating of this second messenger gated channel could then be described by a Markov model, such as the following two-state model,

$$C + Z \underset{\longleftarrow}{\longrightarrow} O \tag{43}$$

or by a more complex multi-state model. For example, Destexhe et al.[26] found that a four-state Markov model was needed to adequately fit both the rising and decaying phases of a G-protein-activated $GABA_B$ receptor current.

## Multicompartment Models

A simple electrical equivalent circuit, such as that shown in Figure 1, can be used to model a localized region of nerve cell membrane. In general, however, neurons have spatially extended axons and dendrites with heterogeneous properties. Different regions of the cell will have different diameters and varying types and densities of ion channels and receptors. Furthermore, quantities such as the local membrane potential and the local intracellular calcium concentration can vary significantly across the spatial extent of a neuron. Multicompartment models provide a means for handling the spatial complexity of neuron morphology and the heterogeneity of physical properties. Figure 9 illustrates the compartmental modeling approach for

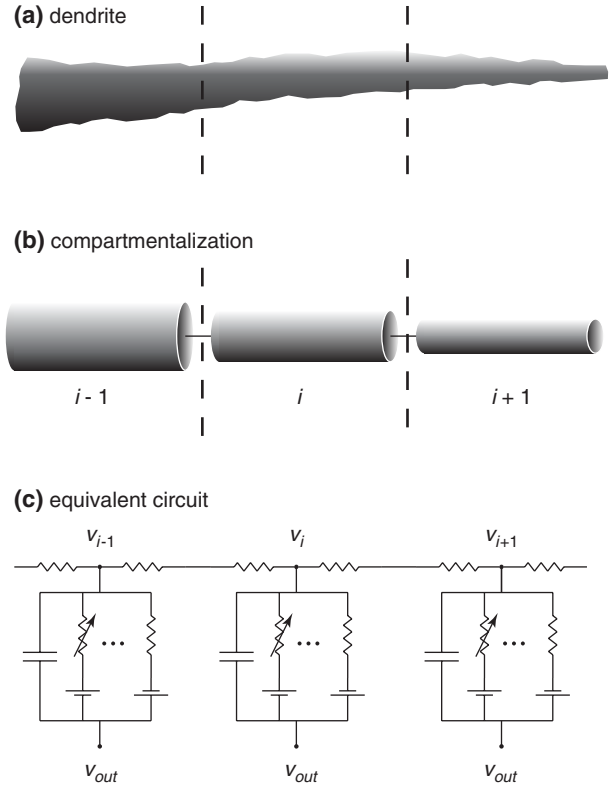


**FIGURE 9** | Compartmental approach for single-neuron modeling. The dendrites (a) are divided into distinct regions that are represented by cylindrical compartments (b). Each compartment can have different physical characteristics (membrane potential, length, diameter, channel types, channel densities, etc.). The physical properties are modeled by an electrical equivalent circuit (c). In the circuit model, neighboring compartments are coupled by resistors representing the axial resistance of the intracellular space. Branch points are handled in a similar manner (data not shown).

a segment of dendritic membrane. The multicompartment modeling approach divides the neuron into a number of smaller spatial compartments, each of which can be modeled with an electrical equivalent circuit similar to Figure 1. The components of the equivalent circuit and their numerical values can vary from compartment to compartment, depending on the particular types of conductances found in different regions of the cell. Neighboring compartments are coupled by axial currents that flow between compartments in the intracellular space. The membrane potential for compartment $i$, $V_i$, is related to the membrane potentials in neighboring compartments, $V_{i-1}$ and $V_{i+1}$, by

$$C_m \frac{dV_i}{dt} + I_{ion} = \frac{(V_{i-1} - V_i)}{r_{i-1,i}} + \frac{(V_{i+1} - V_i)}{r_{i+1,i}} \quad (44)$$

where $C_m$ and $I_{ion}$ are based on the equivalent circuit for compartment $i$. The terms $r_{i\pm1,i}$ represent the axial resistances between neighboring compartments, and the terms $(V_{i\pm1,i} - V_i)/r_{i\pm1,i}$ represent the axial currents. Similar relationships exist for branch points where an axonal or dendritic segment splits into two or more subsegments. Using these techniques, multicompartment models can describe arbitrarily complex cell morphologies. Detailed advice on how to construct, parameterize, and test multicompartment models can be found in Refs 28, 29 and 37.

## Network Models

Previous sections have covered techniques for modeling single neurons, ion channels, and individual synapses. Using these techniques, it is relatively straightforward to create network models, in which the spike outputs from certain model neurons provide synaptic inputs to other neurons in the network. There are two main issues to consider in constructing network-level models. One involves choosing an appropriate mathematical representation for the propagation of action potentials between neurons. The other issue has to do with techniques for specifying the synaptic connectivity within the network.

In principle, the propagation action potentials between neurons could be handled using HH conductances and a multicompartmental description of the axon and its terminal arbor. This approach is sometimes used when the scientific questions being addressed pertain explicitly to mechanisms of action potential propagation.[30] However, it is computationally expensive to use a full multicompartment model to describe every axon and terminal arbor in a large network. Because of the all-or-none nature of the action potential, it is often possible to use a more efficient technique in which action potentials are represented as discrete temporal events. In this event-based approach, an action potential generated by neuron $i$ at time $t_i$ is represented as a time-stamped event that is used to trigger synaptic input to a target neuron $j$ after some time delay $\Delta t_{ij}$. Propagation along the axon is not modeled explicitly; rather it is implicit in the axonal propagation delay $\Delta t_{ij}$. Recall that a single axon typically makes synaptic contacts with multiple target neurons. In general, the propagation delay $\Delta t_{ij}$ can have different numerical values for each of the possible postsynaptic targets.

The second issue in network modeling involves specification of the connectivity between neurons. For small network models, this is often handled on a case-by-case basis, whereas large network models usually require a rule-based approach. For example, a model of an invertebrate central pattern generator might involve 10 neurons with an average of five synapses per neuron, resulting in approximately 50 synaptic connections. Specification of the synaptic properties (receptor type, reversal potential, peak conductance, propagation delay, etc.) could easily be handled on a synapse-by-synapse basis. In contrast, a network model of a local region of mammalian visual cortex might involve on the order of 10,000 neurons with an average of 100 synapses per neuron, resulting in one million synaptic connections. In this case, a synapse-by-synapse specification would be unfeasible and a rule-based approach would be utilized. For example, a connection rule might specify that all neurons of type $A$ (e.g., inhibitory interneurons) make a particular type of synaptic connection (e.g., GABAergic) with all neurons of type $B$ (e.g., pyramidal cells) that lie within a fixed radius. The rule might also specify how the peak conductance and axonal propagation delay vary with target distance.

## Software Tools

Fortunately, sophisticated software packages are available to facilitate the development, implementation, and dissemination of biophysically detailed neural models. Two of the most widely used tools are GENESIS (GEneral NEural SImulation System)[32,33] and NEURON.[34] Both of these modeling environments are designed for constructing biophysically detailed multicompartment models of single neurons, and they also provide modeling tools that span from the molecular level to the network level. Both GENESIS and NEURON provide high-level languages for model specification, predefined sets of neural building blocks, and graphical user interface elements for simulation control and visualization. To construct a

  

specific neural model, the model specification language is used to define and link appropriate sets of predefined building blocks to create a functional model. The basic building blocks include such things as compartments or cable segments for modeling neuron morphology, voltage-gated and ligand-gated conductances, components for intracellular diffusion and buffering of ions, chemical and electrical synapses, and various forms of synaptic plasticity. Other building blocks provide the model with external inputs and outputs, including file I/O and graphical displays. Some building blocks provide models of electrophysiological instrumentation like stimulus generators and voltage-clamp circuits, which allow users to closely model the experimental setups that are used in empirical studies. Custom user-defined elements can be created if the required modeling component is not already part of the predefined set of building blocks. More information on these modeling environments, including documentation, tutorials, users groups, and workshop announcements, can be found on the Web by following the links provided in the Web Resources section.

## CURRENT APPLICATIONS

Hundreds of biophysically detailed neural models have been developed using GENESIS, NEURON, and similar modeling tools. The scientific issues addressed in these models span a broad range of topics, including intracellular signaling, dendritic processing, neural oscillations, central pattern generation, motor control, sensory coding, feature extraction, learning, and memory. See the 'Web Resources' section for links to research publications that have been generated using GENESIS and NEURON. An illustrative example of this type of biophysically detailed modeling approach is provided by the cerebellar Purkinje cell model developed by De Schutter and Bower[31,35] using GENESIS. The dendritic morphology shown in Figure 10 contains approximately 1600 distinct compartments with lengths and diameters based on detailed anatomical reconstructions of an actual Purkinje cell.[36] The model includes 10 different types of voltage-dependent channels: two $Na^+$ channels (fast and persistent), two $Ca^{2+}$ channels (T-type and P-type), three voltage-dependent $K^+$ channels, and two $Ca^{2+}$-dependent $K^+$ channels. The channel properties were modeled using HH equations, and the modeling parameters were constrained by empirical voltage-clamp data where available. The channels were distributed differentially over three zones of the Purkinje cell. Synaptic inputs were modeled using a dual exponential version of the alpha function [Eq. (35)] that allows for different time constants for the rising and falling phases of the synaptic waveform.[23] Figure 10 shows the response of the model to a large synchronous synaptic activation over a large portion of the dendritic tree. This pattern of synaptic input represents activation of the Purkinje cell by a climbing fiber input. The so-called 'complex spike' response of a Purkinje cell to climbing fiber stimulation has been well studied experimentally. The ability of the model to reproduce known membrane voltage and intracellular calcium characteristics of a complex spike was one of the benchmarks for tuning certain model parameters and for evaluating the underlying modeling assumptions. The simulation results summarized in Figure 10 represent only one of several studies carried out using the Purkinje cell model.[31,35] After tuning the model to reproduce a range of *in vitro* firing behaviors, the model was used to make predictions about the *in vivo* firing patterns of Purkinje cells. The model has been particularly useful in elucidating the role of dendritic inhibition in shaping neural response properties.

## LIMITATIONS

There are several limitations to keep in mind when developing biophysically detailed neural models. Perhaps one of the most important is that such models are actually highly impoverished relative to the true richness and complexity of the underlying biology. Even though these models are described as 'biophysically detailed', many aspects of cell and membrane physiology have been stripped away in the modeling process. The art of creating a good model involves knowing which details are important and which details can be safely disregarded. However, details that are unimportant in one functional context may become pivotal in a different context. Thus, one should avoid thinking of any particular model, such as the Purkinje cell model described above, as a full and complete description of the underlying biological system.

It is better to think of a neural model as an extended hypothesis that is designed to address a restricted range of neurobiological function. As an extended hypothesis, each model embodies a large number of assumptions. Certain assumptions will be well supported by empirical data, while others will be largely speculative. For the purpose of hypothesis testing, it is important to keep track of all the underlying assumptions and the corresponding empirical constraints on those assumptions. This is one area where neuroinformatics tools can play a key role in helping modelers establish and document links

  

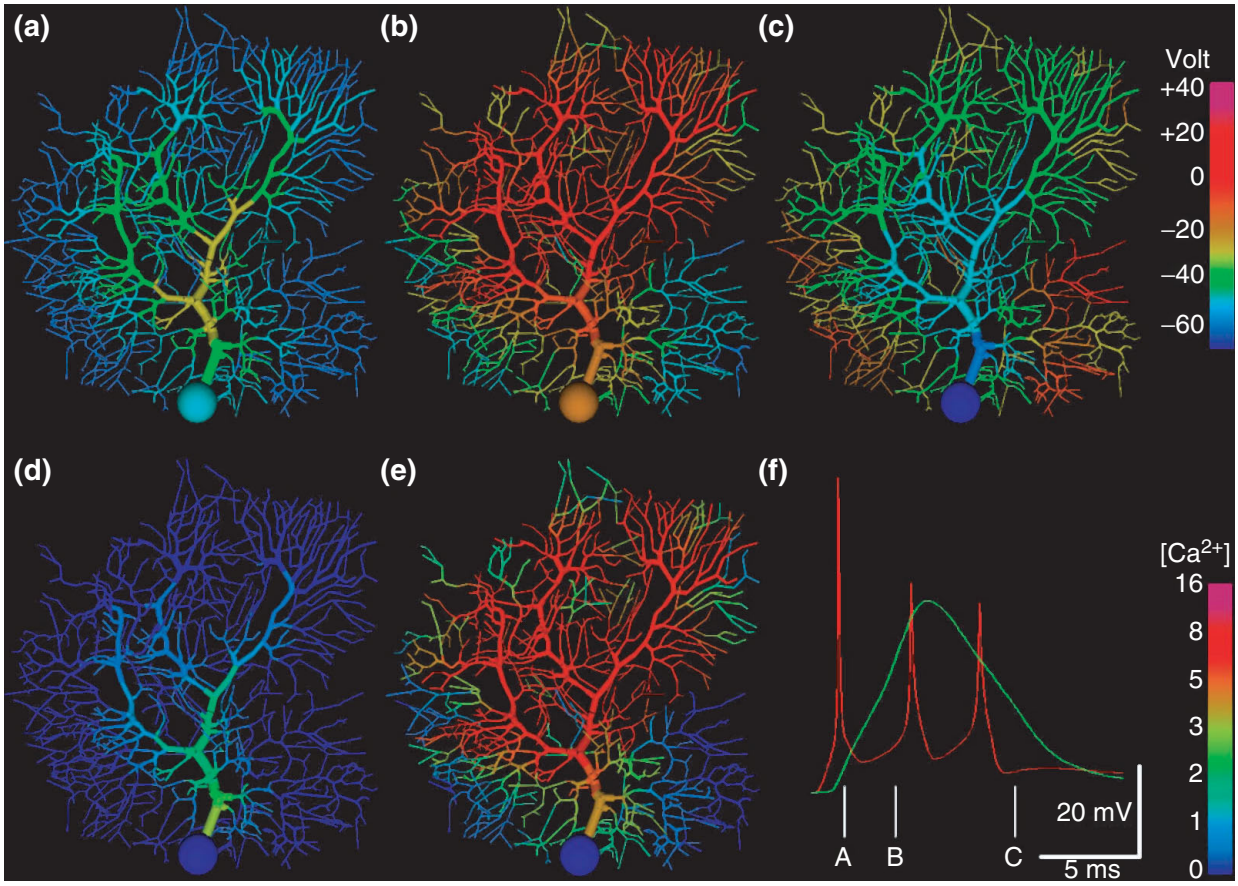


**FIGURE 10** | Representations of the membrane potential and calcium concentration in a large compartmental model of a cerebellar Purkinje cell following synaptic activation. (a–c) Membrane potential 1.4, 4.0, and 10.0 ms after synaptic activation. (D and E) Intracellular $Ca^{2+}$ concentration 1.4 and 4.0 ms after activation. (f) Membrane potential (red trace) and $Ca^{2+}$ concentration (green trace) in the cell body following activation. The vertical white bars indicate the times at which the false color images in panels (a)–(e) were generated. (Adapted with permission from Ref 31. Copyright 1994 John Wiley & Sons, Inc.).

between each assumption and the set of empirical results that impact that particular assumption. In terms of hypothesis testing, an important limitation to keep in mind is that even if a neural model successfully reproduces certain empirical results, it does not imply that all the underlying assumptions in the model are true. Likewise, if a model fails to agree with some piece of empirical data, the fact that the 'extended hypothesis' is falsified does not directly indicate which of the underlying assumptions might be responsible for the disagreement. Therefore, it is not particularly useful to simply label a neural model as 'right' or 'wrong'. Instead, neural modeling should be viewed as an integral component of the scientific method, in which progress is made through multiple iterations of experimental observation, hypothesis generation (model building), prediction (model simulation), and testing (comparison with empirical data).

## OUTLOOK

Based on research trends over the past decade, it is clear that both neuroinformatics and electrophysiological modeling are becoming increasingly important tools for exploring the functional properties of neural systems. Several ongoing research and development efforts are leading toward a convergence and integration of neuroinformatics and modeling tools that will greatly enhance the ability of neuroscientists to make use of these powerful approaches. Much of this development effort is taking place in the context of the Human Brain Project.[3–5] Several research groups are actively developing large electrophysiological databases, common data representations to facilitate information sharing, software tools for electrophysiological data analysis and visualization, neuroinformatics tools for search and retrieval, and neuroinformatics-based extensions to neural modeling software packages.

  

## REFERENCES


1. Koch C, Segev I, eds. *Methods in Neuronal Modeling: From Ions to Networks*. 2nd ed. Cambridge, MA: MIT Press; 1998.
2. De Schutter E, ed. *Computational Neuroscience: Realistic Modeling for Experimentalists*. Boca Raton, FL: CRC Press; 2001.
3. Huerta MF, Koslow SH, Leshner AI. The Human Brain Project: an international resource. *Trends Neurosci* 1993, 16:436–438.
4. Koslow S, Huerta M, eds. *Neuroinformatics: An Overview of the Human Brain Project*. Mahwah, NJ: Erlbaum; 1997.
5. Shepherd GM, Mirsky JS, Healy MD, Singer MS, Skoufos E, et al. The Human Brain Project: Neuroinformatics tools for integrating, searching, and modeling multidisciplinary neuroscience data. *Trends Neurosci* 1998, 21:460–468.
6. Rudy B. Diversity and ubiquity of K channels. *Neuroscience* 1988, 25:729–749.
7. Coetzee WA, Amarillo Y, Chiu J, Chow A, Lau D, et al. Molecular diversity of $K^+$ channels. *Ann N Y Acad Sci* 1999, 868:233–285.
8. Rudy B, Chow A, Lau D, Amarillo Y, Ozaita A, et al. Contributions of Kv3 channels to neuronal excitability. *Ann N Y Acad Sci* 1999, 868:304–343.
9. Rashid AJ, Dunn RJ, Turner RW. A prominent soma-dendritic distribution of Kv3.3 $K^+$ channels in electrosensory and cerebellar neurons. *J Comput Neurol* 2001, 441(3):234–247.
10. Rashid AJ, Morales E, Turner RW, Dunn RJ. The contribution of dendritic Kv3 $K^+$ channels to burst discharge in a sensory neuron. *J Neurosci* 2001, 21(1):125–135.
11. Doiron B, Longtin A, Turner RW, Maler L. Model of gamma frequency burst discharge generated by conditional backpropagation. *J Neurophysiol* 2001, 86:1523–1545.
12. Wang L-Y, Gan L, Forsythe ID, Kaczmarek LK. Contribution of the Kv3.1 potassium channel to high-frequency firing in mouse auditory neurons. *J Physiol (London)* 1998, 509:183–194.
13. Delcomyn F. *Foundations of Neurobiology*. New York: Freeman; 1998.
14. Shepherd GM. *Neurobiology*. 3rd ed. New York: Oxford University Press; 1994.
15. Levitan IB, Kaczmarek LK. *The Neuron: Cell and Molecular Biology*. 3rd ed. New York: Oxford University Press; 2002.
16. Hille B. *Ion Channels of Excitable Membranes*. 3rd ed. Sunderland, MA: Sinauer; 2001.
17. Hodgkin AL, Huxley AF. A quantitative description of membrane current and its application to conduction and excitation in nerve. *J Physiol (London)* 1952, 117:500–544.
18. Traub RD. Simulation of intrinsic bursting in CA3 hippocampal neurons. *Neuroscience* 1982, 7:1233–1242.
19. Yamada W, Koch C, Adams P. Multiple channels and calcium dynamics. In: Koch C, Segev I, eds. *Methods in Neuronal Modeling: From Synapses to Networks*. 2nd ed. Cambridge, MA: MIT Press; 1998, 137–170.
20. Destexhe A, Huguenard J. Which formalism to use for modeling voltage-dependent conductances? In: De Schutter E, ed. *Computational Neuroscience: Realistic Modeling for Experimentalists*. Boca Raton, FL: CRC Press; 2001, 129–157.
21. Patlak JB. Molecular kinetics of voltage-dependent $Na^+$ channels. *Physiol Rev* 1991, 71:1047–1080.
22. Rall W. Distinguishing theoretical synaptic potentials computed for different soma-dendritic distributions of synaptic input. *J Neurophysiol* 1967, 30:1138–1168.
23. Wilson MA, Bower JM. The simulation of large-scale neuronal networks. In: Koch C, Segev I, eds. *Methods in Neuronal Modeling: From Synapses to Networks*. Cambridge, MA: MIT Press; 1989, 291–334.
24. Srinivasan R, Chiel HJ. Fast calculation of synaptic conductances. *Neural Comput* 1993, 5:200–204.
25. Destexhe A, Mainen ZF, Sejnowski TJ. Kinetic models of synaptic transmission. In: Koch C, Segev I, eds. *Methods in Neuronal Modeling: From Ions to Networks*. 2nd ed. Cambridge, MA: MIT Press; 1998, 1–26.
26. Destexhe A, Mainen ZF, Sejnowski TJ. Synthesis of models for excitable membranes, synaptic transmission and neuromodulation using a common kinetic formalism. *J Comput Neurosci* 1994, 1:195–230.
27. Bhalla US. Modeling networks of signaling pathways. In: De Schutter E, ed. *Computational Neuroscience: Realistic Modeling for Experimentalists*. Boca Raton, FL: CRC Press; 2001, 25–48.
28. Segev I, Burke RE. Compartmental models of complex neurons. In: Koch C, Segev I, eds. *Methods in Neuronal Modeling: From Ions to Networks*. 2nd ed. Cambridge, MA: MIT Press; 1998, 63–96.
29. De Schutter E, Steuber V. Modeling simple and complex active neurons. In: De Schutter E, ed. *Computational Neuroscience: Realistic Modeling for Experimentalists*. Boca Raton, FL: CRC Press; 2001, 233–257.
30. Manor Y, Gonczarowski J, Segev I. Propagation of action potentials along complex axonal trees: model and implementation. *Biophys J* 1991, 60:1411–1423.


  

31. De Schutter E, Bower JM. An active membrane model of the cerebellar Purkinje cell: II. Simulation of synaptic responses. *J Neurophysiol* 1994, 71:401–419.
32. Bower JM, Beeman D, eds. *The Book of GENESIS: Exploring Realistic Neural Models with the GEneral NEural SImulation System*. New York: Springer-Verlag; 1998.
33. Bower JM, Beeman D, Hucka M. GENESIS simulation system. In: Arbib MA, ed. *The Handbook of Brain Theory and Neural Networks*. 2nd ed. Cambridge, MA: MIT Press; 2002, 475–478.
34. Hines ML, Carnevale NT. NEURON simulation environment. In: Arbib MA, ed. *The Handbook of Brain Theory and Neural Networks*. 2nd ed. Cambridge, MA: MIT Press; 2002, 769–773.
35. De Schutter E, Bower JM. An active membrane model of the cerebellar Purkinje cell I. Simulation of current clamps in slice. *J Neurophysiol* 1994, 71:375–400.
36. Rapp M, Yarom Y, Segev I. The impact of parallel fiber background activity on the cable properties of cerebellar Purkinje cells. *Neural Comput* 1992, 4:518–533.
37. Segev I. Cable and compartmental models of dendritic trees. In: Bower JM, Beeman D, eds. *The Book of GENESIS: Exploring Realistic Neural Models with the GEneral NEural SImulation System*. New York: Springer-Verlag; 1998, 51–77.

## WEB RESOURCES

CATACOMB: a simulation system for biologically based network models (http://www.compneuro.org/catacomb/)

GENESIS: a general-purpose simulation system for single neuron and network models (http://www.genesis-sim.org/GENESIS/). For a list of research publication using the GENESIS simulator, see http://www.genesis-sim.org/GENESIS/pubs.html

NEURON simulator: a general-purpose simulation system for single neuron and network models (http://www.neuron.yale.edu/). For a list of research publication using the NEURON simulator, see http://www.neuron.yale.edu/neuron/bib/usednrn.html

NeuroML: a prototype markup language for describing neuroscience simulation models (http://www.neuroml.org/)

SenseLab: prototype databases of cell properties, membrane properties, and neural models (http://senselab.med.yale.edu/senselab/)

  